Petroleum Science 18 (2021) 1739–1752

Contents lists available at ScienceDirect

Petroleum Science

journal homepage: www.keaipublishing.com/en/journals/petroleum-science

Original Paper

Near-wellbore fracture initiation and propagation induced by drilling fluid invasion during solid fluidization mining of submarine nature gas hydrate sediments

Hai-Yan Zhu [a], Yi-Ke Dang [b, c], Guo-Rong Wang [c, *], Shou-Wei Zhou [d], Qiang Fu [d]

[a] State Key Laboratory of Oil and Gas Reservoir Geology and Exploitation, Chengdu University of Technology, Chengdu, 610059, Sichuan, China
[b] School of Human Settlements and Civil Engineering, Xi'an Jiaotong University, Xi'an, 710049, Shaanxi, China
[c] School of Mechatronic Engineering, Southwest Petroleum University, Chengdu, 610500, Sichuan, China
[d] China National Offshore Oil Corporation, Beijing, 100010, China

ARTICLE INFO

Article history:
Received 11 November 2020
Accepted 5 March 2021
Available online 20 September 2021

Edited by Yan-Hua Sun

Keywords:
Near wellbore
Crack initiation and propagation
Drilling fluid invasion
Natural gas hydrate
Wellbore instability

ABSTRACT

Drilling in a natural gas hydrate formation is challenging due to the poor consolidation of the formation and the potential evaporation of the hydrate. The unreasonable down-hole pressure of the drilling fluid can not only lead to the wellbore instability, but also change the predrilling condition of the natural gas hydrate formation, thus leading to an instable wellbore. In this paper, the integrated discrete element method (DEM)-computational fluid dynamics (CFD) work flow is developed to study the wellbore instability due to the penetration of the drilling fluid into the hydrate formation during crack propagations. The results show that the difference between in-situ stresses and overpressure directly affect the drilling fluid invasion behavior. The lower hydrate saturation leads to an easier generation of drilling fluid flow channels and the lower formation breakdown pressure. The breakdown pressure increases with the increase of hydrate saturation, this also indicates that hydrates can enhance the mechanical properties of the formation. The induced cracks are initially accompanied with higher pressure of the drilling fluid. According to the rose diagram of the fracture orientation, a wider orientation of the fracture distribution is observed at higher pressure of the invasion fluid.

1. Introduction

The permafrost area of Qinghai-Tibet plateau and the South China Sea are rich in natural gas hydrate resource. Due to the harsh drilling environment and the delicate environment of natural gas hydrates, the wellbore instability is one of the major problems encountered during drilling. In the drilling process, the drilling fluid tends to invade the hydrate formation under the overpressure in the well. If the temperature of the drilling fluid is higher than the original temperature of the formation, and the hydrates will decompose (Sloan, 2003; Zhu et al. 2011, 2013, 2013; Wang et al., 2020). Moreover, the water generated from the decomposition of hydrates will increase the water content of the formation around the borehole wall, leading to the weakening of the boundaries between the particles, which will affect the distribution of rock stress field around the borehole and then it will cause the instability of the borehole. In addition, due to the poor consolidation condition of the hydrate formation, then drilling fluid will invade the hydrate formation under the overbalanced pressure and then change the preexisting pressure environment of natural gas hydrates, accelerating the borehole wall instability. Therefore, the study of wellbore stability in the hydrate zone is necessary and useful.

Freij-Ayoub et al. (2007) established a numerical model for analyzing hydrate wellbore stability. The simulation results show that when the drilling fluid temperature is 5 °C higher than that of the reservoir, the yield zone around the wellbore will expand by 32%. Khabibullin et al. (2011) proposed a numerical model for predicting the temperature field around the well, and found that the decomposition amount of hydrates depends on the initial characteristics of the reservoir and the formation temperature and pressure conditions. According to the work of Wojtanowicz et al.

---

* Corresponding author.
E-mail address: 200331010023@swpu.edu.cn (G.-R. Wang).

https://doi.org/10.1016/j.petsci.2021.09.026

(2000), there is no vertical fracture induced in the shallow zone, while the horizontal fracture is the main reason for the lost circulation. Chong et al. (2018) used experimental equipment to study the influence of horizontal well mining method on reducing pressure during hydrate evaporation, and found that the horizontal well mining method can increase gas production and reduce water production. Birchwood et al. (2007) found that mud circulation rate is the most critical factor to maintain hydrate stability. The simulation results by Li et al. (2011) show that the thermal decomposition of hydrate will lead to the deterioration of mechanical properties of the reservoir. Rutqvist et al. (2012) found that gas production rate and bottom hole pressure drop determine the pressure state of the entire reservoir and change the mechanical state of the reservoir near the well zone. Sun et al. (2018) carried out numerical analysis for the wellbore stability in the hydrate layers of the Shenhu sea area in the South China Sea. The results show that the thermal effect induced by the temperature difference between the drilling fluid and the formation and the high salinity of the drilling fluid can cause the release of free gas in the reservoir, resulting in an increase in pore pressure in the near-well zone. And proper salinity of the drilling fluid can effectively control the generation of free gas and prevent wellbore instability.

The literature review about wellbore stability in hydrate formation indicates that many theories have been proposed, and some important factors such as temperature change and borehole pressure were investigated. However, the study on dynamic characteristics of drilling fluid invasion into the hydrate formation and its influence on the formation stresses are seldom conducted. The previous studies also shown that the stability of borehole in the drilling process has closely related to the physical parameters of the hydrate formation (Freij-Ayoub, 2008; Ning et al., 2013b). There is few quantitative research on reservoir mechanical response, especially the mechanical response of the formation around the borehole.

In addition, the drilling fluid plays an important role during drilling, during drilling a hydrate formation, there are usually differences in temperature and pressure between the formation and the borehole. Therefore, after the borehole is opened and the drilling fluid contacts with the hydrate formation, it is very easy to invade the formation and may break the phase equilibrium conditions of hydrate in situ, resulting in hydrate decomposition, which increases to the risk of wellbore instability (Ning et al., 2013a, 2013b, 2013b; Sun et al., 2015). The current research is mainly focused on the drilling fluid after it intrudes into the formation, the variation of pore pressure around the well and the mechanical strength induced by hydrate decomposition (McConnell et al., 2012; Merey, 2016). However, there are few reports on the invasion mode of the drilling fluid into the formation and the flow law of the drilling fluid after formation rupture. Therefore, combined with the above discussion, it is particularly important to investigate the dynamic characteristics of drilling fluid invasion into the formation, the way of drilling fluid invasion into the formation and the flow law after the invasion.

Hydraulic fracturing is an important technology in gas/oil exploitation (Nasehi and Mortazavi, 2013), mining engineering (Li, 2014), geothermal engineering (Pogacnik et al., 2016), in situ stress measurements (Liu et al., 2014; Wang et al., 2015) and more. The particle flow theory is a mature discrete element method, which is suitable for solving large deformation problems of solid mechanics and flow problems of granular media. Many scholars have studied hydraulic fracturing using particle discrete element method. Yoon et al. (2014, 2015) established a water-force coupling model and used the DEM to study the influence of hydraulic fracturing on the stimulation of natural fractures in deep reservoirs and the change of stress state of fractures induced by fluid injected into geothermal reservoirs with natural fractures. Liu et al. (2015) studied the crack propagation induced by fluid injected into particle flow materials by particle flow method. Shimizu et al. (2011) simulated the hydraulic fracturing with the DEM. It was found that the smaller the viscosity coefficient, the faster the pressure diffusion, and the numerical results agree well with the experimental results.

In this study, based on DEM method, a coupled fluid-solid coupling model was built to investigate the dynamic characteristics of drilling fluid invasion into the formation, the way of drilling fluid invasion into the formation from the perspective view of near-wellbore crack initiation and propagation.

2. Coupled DEM-CFD theory of crack initiation and propagation

2.1. Fluid flow equations

For the DEM (Itasca Consulting Group, 2008), the following assumptions are made in fluid-solid coupling:

(1) It is assumed that there is a sensitive unit in the model that can store pressure, called a domain, as shown in the black line in Fig. 1, and adjacent channels are connected by a seepage channel.
(2) It is assumed that the seepage path of the fluid is formed by the parallel plate channels between the particles, which is called the "seepage channel" as shown in Fig. 2.

The pore fluid is stored in pore grids (domains). Fluid exchange occurs in adjacent pore grids under the pressure gradient. To calculate the flow rate of the fluid exchange, it is assumed that the fluid passage is a parallel plate passage between two adjacent particles (Fig. 2) The dimensions of the local flow path are length, L, opening/width a, and unit thickness. Then, the flow between the two pores can be expressed by the Hagen-Poiseuille equation (Berman, 1953):

$$q = ka^3 \frac{P_2 - P_1}{L} \tag{1}$$

where q is the flow rate, a is the opening/width of the percolation

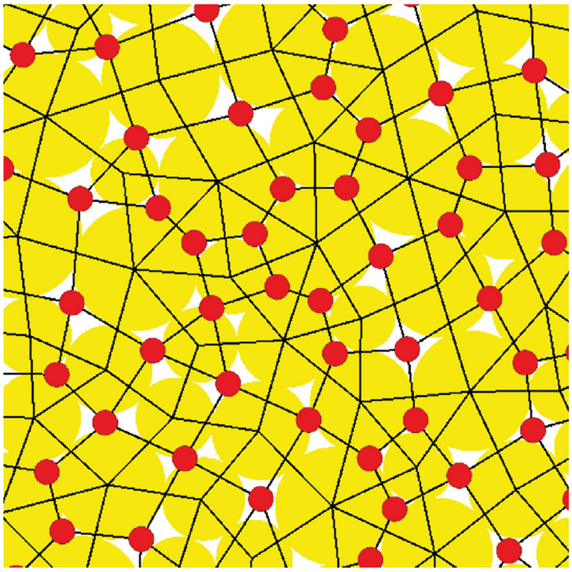

Fig. 1. Schematic diagram of the domain (Duan et al., 2018).

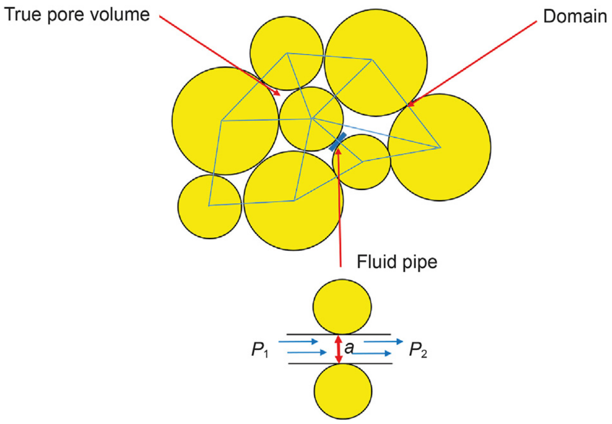

Fig. 2. Schematic diagram of the seepage channel (Huang et al., 2019).

passage, which is dependent on the normal force of the two particles, k is the permeability coefficient, L is the length of the flow path, P_1 is the inlet pressure and P_2 is the outlet pressure (Fig. 2).

It can be seen from the above formula that the opening a will affect the flow dramatically. The influence of the mechanical process on the fluid flow is mainly reflected in the fact that it dominates the opening of the pore channel. While the fluid flow will introduce fluctuation of the pore fluid pressure, and viscous force of the particles and the fluid flow. It is assumed that when the contact force between the particles is zero, the corresponding opening of the channel is a_0 which is called the residual opening.

When the normal contact force is in tension, the opening is equal to the sum of the residual opening and the normal distance between the surface of the two particles (the normal distance should be multiplied by the scaling factor m) (Lönnqvist and Hökmark, 2016):

$$a = a_0 + mg \tag{2}$$

where g is the normal distance between the surfaces of the two particles, m is a dimensionless multiplier.

When the normal contact force between the two particles is compressive, the opening of the fluid channel is expressed as (Itasca Consulting Group, 2008):

$$a = \frac{a_0 F_0}{F + F_0} \tag{3}$$

where F_0 is the value of normal force at which the aperture decreases to $a_0/2$, and F is the normal contact force under the current load.

From Eq. (2), as the compression force between particles increases or decreases, the opening will correspondingly decrease or increases. Hydraulic coupling is achieved by the relationship of force and the opening of a flow path.

When two cemented particles are in tension or the bond between two particles has been broken, the opening a when the particles are broken at the contact point is (Itasca Consulting Group, 2008):

$$a = a_0 + \lambda(d - R_1 - R_2) \tag{4}$$

where d is the distance between two particles, R_1 and R_2 are the radius of the two particles, respectively, and λ is a dimensionless multiplier. For most models, the particle size is much larger than the actual particle size, and the calculated opening will also be larger. Therefore, a constant less than 1 of λ is often applied to obtain a reasonable opening.

2.2. Pore pressure equation

During the time increment of Δt, the change of pore fluid pressure due to fluid flow in/out is calculated with the volumetric compressive modulus of the fluid. Consider a certain pore, which has N channels for fluid flow in and out, the total flow of the fluid is $\sum q$, and the change of the pore fluid pressure could be obtained as (Itasca Consulting Group, 2008):

$$\Delta P = \frac{K_f}{V_d}\left(\sum q\Delta t - \Delta V_d\right) \tag{5}$$

where K_f is the fluid bulk modulus, V_d is the apparent volume of the domain, $\sum q$ is the total flow rate obtained by the domain from the surrounding domains, and ΔV_d is the volume change of the domain caused by force.

2.3. Fluid-solid coupling process

There are three main mechanisms of interaction between particles and fluid in discrete elements:

(1) Change of flow path through opening and closing of the contact status between the particles or the change in contact force;
(2) Change of the domain pressure due to the mechanical changes in domain volumes;
(3) The domain pressure has traction on the closed particles.

In the above three mechanisms, the first two have been considered by Eqs. (2)–(5). For the last mechanism one, it is assumed that the fluid pressure in the domain is evenly distributed along the lines between the surrounding contacts (black line segments in Fig. 2).

According to the above assumptions, the fluid action and the seepage pressure on the particles can be expressed as (Itasca Consulting Group, 2008), Fig. 3 shows the pressure distribution in a single domain. The osmotic pressure acting on the ball will change during the calculation, which also changes the fluid pressure in the domain. The fluid pressure can be expressed as,

$$f_i = P_f L_i t \tag{6}$$

where f_i is the fluid pressure acting on each ball, L_i is the distance between two contact points on the same particle (the red line

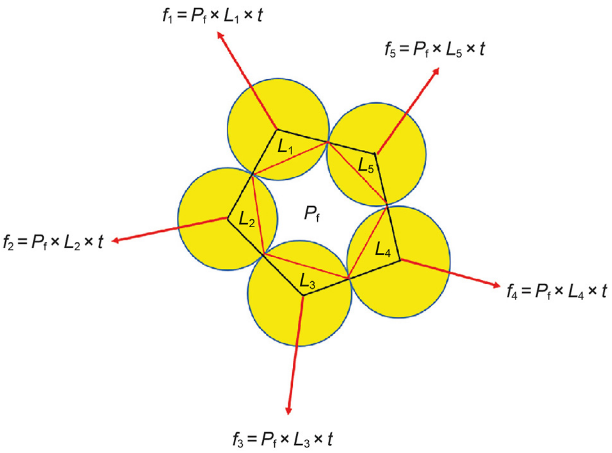

Fig. 3. Pressure distribution in the domain (Zhou et al., 2016).

shown in Fig. 3), t is the current time step and P_f is the fluid pressure in the single domain.

2.4. Seepage calculation time step

In order to ensure the stability of the seepage calculation, its time step should not exceed the critical value. Assuming that there is a pressure disturbance in a domain, the flow into the domain due to the disturbance can be derived from Eq. (1) and expressed as follows (Itasca Consulting Group, 2008):

$$q = \frac{Nka^3\Delta P_P}{2R} \tag{7}$$

where R is the average radius of the particles surrounding the domain and N is the number of channels connected to the domain, ΔP_p is pressure change in a single domain, q is the flow rate in the parallel plate pipe.

Then, according to Eq. (5), the pressure increment generated by the flow in the domain can be obtained as follows:

$$\Delta P_r = \frac{K_f q \Delta t}{V_d} \tag{8}$$

where P_r is the pressure increase.

To maintain the stability of seepage calculation, the pressure caused by the perturbed flow must be less than the perturbed pressure. When the two are equal, the critical time step can be obtained from Eqs. (7) and (8):

$$\Delta t = \frac{2RV_d}{NK_f ka^3} \tag{9}$$

In order to ensure the stability of the whole domain, the global time step must be the product of the minimum value among all the local time steps and a safety factor less than 1.0.

3. Numerical model set up

The particle flow code (PFC) is a particle flow theory soft raised by Cundall (Cundall and Strack, 1979). In a two-dimensional particle flow code (PFC2D), the basic components are particles and bonds, the solution method is to abstract and simplify the physical model of practical engineering problems, from the micro point of view to establish a mathematical model in line with the characteristics of the project, then, the physical and mechanical parameters, initial conditions and boundary conditions are given to the model, to realize the simulation solution of engineering problems. Discrete particles are rigid particles with normal and shear stiffness with either contact bonds (CB) or parallel bonds (PB) as their two bond modes (Cho et al., 2007; Lisjak and Grasselli, 2014). The parallel bond can transfer force and torque between particles, while a contact bond can only transfer the force acting at the contact point, and cannot transfer the torque. The parallel bonds are more suitable for simulating rock materials. Hence, in the next study, the parallel bonding method will be used for the numerical model.

3.1. Mesoscopic mechanical parameters calibration

In the PFC, when running the simulation tests, a series of microscopic physic-mechanical parameters of the particles and the bond properties are required. However, these parameters cannot be directly acquired from the laboratory tests. Therefore, a set of micro-mechanical parameters needs to be determined before the numerical simulation. In this process, the numerical simulation tests with similar conditions as the laboratory tests were first carried out. Then, the numerical results were compared against the results laboratory. The micro-mechanical parameters were adjusted repeated by "trial and error" method (Castro-Filgueira et al., 2017) until the stress-strain curve of numerical simulation matches the curve of laboratory test, at this point, the micro-mechanical parameters will be determined. It should be noted that the microscopic parameters jointly affect the mechanical characteristics of the sample, so once determined, these parameters are unique, and the micro-mechanical parameters can be used for the following research.

In the current triaxial test simulation with DEM, the servo-testing of the lateral rigid wall is carried out by confining pressure, which will constraint the lateral free deformation of the specimen during the loading process of the confining pressure. On the contrary, the actual triaxial test allows the lateral deformation of the sample cylindrical wall. Therefore, the rigid wall in the DEM cannot reasonably simulate the flexible loading characteristics of the rubber film to the confining pressure in the triaxial experiment. Therefore, based on flexible loading of confining pressure, this paper simulated triaxial tests of natural gas hydrate for parameter calibration.

Fig. 4 is the DEM model during parameter calibration before loading (gray dots represent sand particles, red dots represent hydrate particles, white dots represent pores), and Fig. 5 is the failed samples after loading. The model was generated with a diameter of 50 mm and a height of 100 mm (Zhou et al., 2015) by particles formed in a cylinder consisting of a flexible membrane. The minimum radius of the sand particles is $R_{\text{sand-min}} = 0.3$ mm, and the maximum radius of the sand particles is $R_{\text{sand-max}} = 0.4$ mm. The dimension of the particles obeys the random distribution law. The radius of all the hydrate particles R_{hyd} is 0.2 mm. The density of hydrate is 900 kg/m^3, the density of sand is 2650 kg/m^3 (Zhu et al., 2018), and the porosity of the numerical model is 0.15. Three kinds of contact models were defined in the discrete element model: sand-sand contact, sand-hydrate contact and hydrate - hydrate contact.

In this paper, triaxial test results of hydrated sediment by Yan et al. (2017) were used to verify the proposed discrete numerical model. Through the method of "trial and error" with repeated check comparison, Table 1 lists the available mesoscopic mechanical parameters. Fig. 6 shows that the simulation results have a good agreement with the triaxial test results. This indicates that the

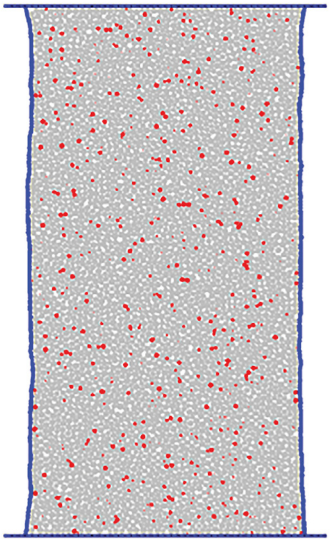

Fig. 4. Triaxial compression test model.

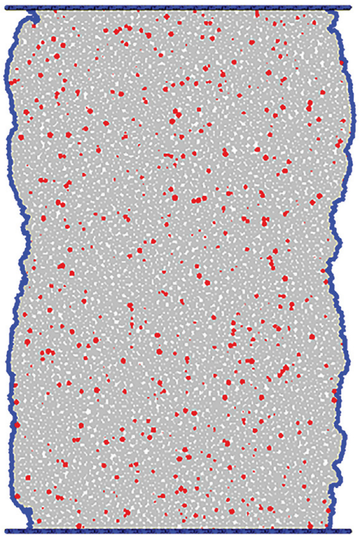

Fig. 5. The end of loading of flexible film.

Table 1
Mesoscopic parameters of the model.

Contact parameters	Sand-sand	Modulus of deformation, MPa	400
		Stiffness ratio	0.7
		Coefficient of friction	0.5
	Sand-hydrate	Modulus of deformation, MPa	400
		Stiffness ratio	0.7
		Coefficient of friction	0.5
	Hydrate-hydrate	Modulus of deformation, MPa	400
		Stiffness ratio	0.7
		Coefficient of friction	0.5
		Tensile strength, MPa	2
		Cohesion, MPa	6
		Internal friction angle, degree	0
Particle parameters	Sand	Density, kg/m^3	2650
		Minimum particle radius, mm	0.3
		Maximum particle radius, mm	0.4
	Hydrate	Density, kg/m^3	900
		Minimum particle radius, mm	0.2
		Maximum particle radius, mm	0.2

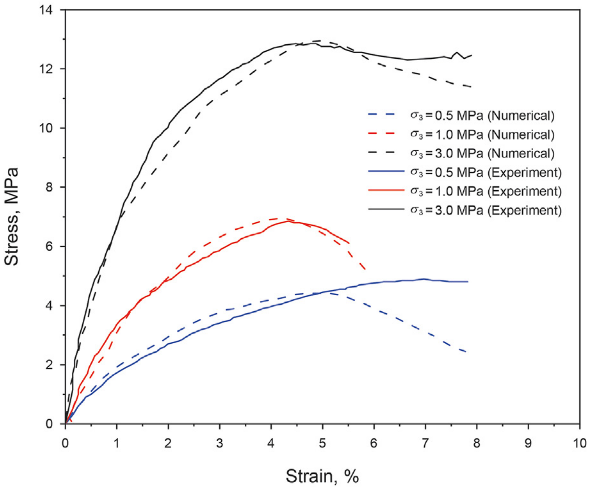

Fig. 6. Verification of numerical simulation results and laboratory experimental results (experimental results from Yan et al. (2017)).

parameters of Table 1 were close to the macroscopic mechanical parameters of the real hydrate sample. Now, the selected mesoscopic parameters can be used for further research below.

3.2. Coupled DEM-CFD model of crack growth in natural gas hydrate formation

Fig. 7 shows the model set by using the PFC2D. The model is 50 mm long and 50 mm high and includes 100 measurement circles that have the diameter of 5 mm. The measurements in the model are intended to record changes in the stress field. In the coupled DEM-CFD model, the minimum radius of the sand particles is $R_{\text{sand-min}} = 0.3$ mm, the maximum radius of the sand particles is $R_{\text{sand-max}} = 0.4$ mm, and the radius of all the hydrate particles $R_{\text{hyd}} = 0.2$ mm. The dimension of the particles obeys the random distribution law and the particle size distribution is consistent with the above. The densities of sand and hydrate are 2650 and 900 kg/m^3, respectively. The porosity of the coupled DEM-CFD model is 0.15. All the boundaries, limited the horizontal movement and the vertical movement. The X direction in the model is set as the direction of the minimum horizontal ground stress and the Y direction is set as the maximum horizontal ground stress. In the middle of the domain, a near circular hole with a diameter of 3 mm was created for water injection. The intrusion of the drilling fluid into the hydrate formation is analyzed by applying uniform and constant water pressure from the water injection hole. In Fig. 7, the blue grid is the channel through which the fluid flows.

3.3. Boundary conditions

The deep-sea shallow hydrate has the characteristics of large reserve and poor cementation, and the formation is a weakly consolidated or unconsolidated non-diagenetic hydrate reservoir. The mining of hydrate reservoirs is often accompanied with high risk of environmental pollution such as large-scale methane escaping and submarine landslides. (Wang et al., 2020). A new method of "solid fluidization mining of submarine hydrate reservoirs" was first proposed by the Marine hydrate development research team headed by academician Zhou, which has significant advantages such as less pollution, less secondary disasters and no

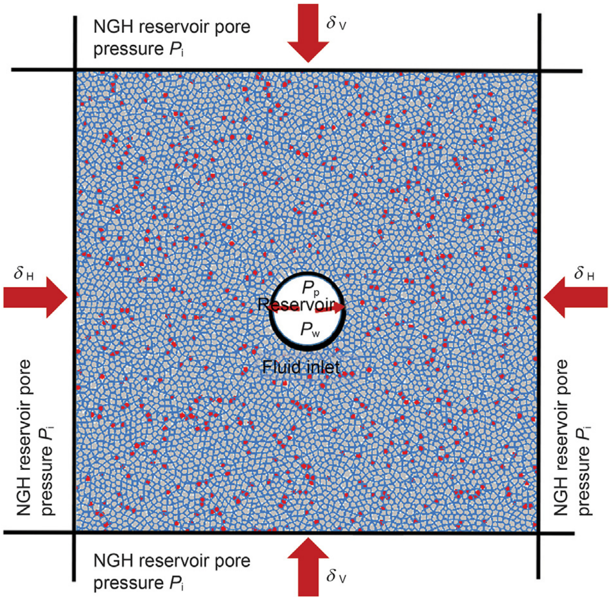

Fig. 7. The coupled DEM-CFD model.

damage to low porosity hydrate reservoirs. Fig. 8 shows two types of wells for “solid fluidization exploitation of shallow hydrates in deep water”.

The first Chinese expedition to drill gas hydrates, GMGS-1, was undertaken in Shenhu area (South China Sea) between April and June 2007. A total of eight sites were drilled and well logged in this survey, with cores recovered at five of these sites, and gas hydrate samples were recovered from three of them. (i.e., site Shenhu-2, Shenhu-3, and Shenhu-7; more details can be found in Wu et al., 2007; Zhang et al., 2007).

Sun et al. (2018) selected the site Shenhu-2 to perform the wellbore stability analysis. Their study details how the in-situ stress, pore pressure and mud stress were calculated in the area. In addition, Zhang et al. (2015) also studied the in-situ stress distribution of the South China Sea, and found that the ratio of the maximum horizontal principal stress to the vertical stress was about 0.76 and the ratio of the maximum to the minimum horizontal principal stress ranged from 1.07 to 1.18.

In this paper, the research background was also based on the Shenhu area (South China Sea), so combining the research results of Sun and Zhang, we choose the parameters in Table 2 to conduct the simulation. The drainage boundary condition was adopted in this proposed discrete element model, the actual stress condition is the effective stress.

3.4. Model verification

Sun et al. (2018) studied the wellbore stabilities of several exploration wells based on the FEM in the Shenhu area of the South China Sea. In order to verify the proposed model in this paper, the obtained numerical simulation results of borehole stability of the formation in this area were compared with the results from Sun et al. using the parameters of Well Shenhu-2. The formation parameters from Well Shenhu-2 and the physical properties of the drilling fluid are shown in Table 3.

Sun et al. calculated the wellbore stability of a vertical well with the same horizontal stresses. The model domain and stress condition were: the radius of the well model is 0.1143 m, the horizontal stress at 217.5 m is 15.74 MPa, and the vertical stress is 16.7 MPa. The analysis model of Sun et al. is show in Fig. 9.

The same dimension and stress condition in Sun's model were applied to our DEM model, and compare the results with Sun et al. (2018). It should be noted that the application of stress in DEM depends on the wall, so a square numerical model is established, this is different from the model of Sun et al. but the two models have the same size. Due to the large geometric size of the established model (Fig. 9), if the same particle size as Fig. 7 is used for modeling, the scale of the model will become very large, which is not realistic.

According to the previous studies, when the ratio between the boundary size and the particle size of the model is greater than a certain value, changing the particle size does not affect the calculation results. Hofmann et al. (2015) and Bahrani et al. (2014) found that the ratio between the height of sample and the particle radius is greater than 60, the particle size has a slight effect on the calculation results. Liu (2017) believes that the ratio between the minimum boundary size of the model and particle radius is greater than 22.8, the particle does not affect the simulation results. It has

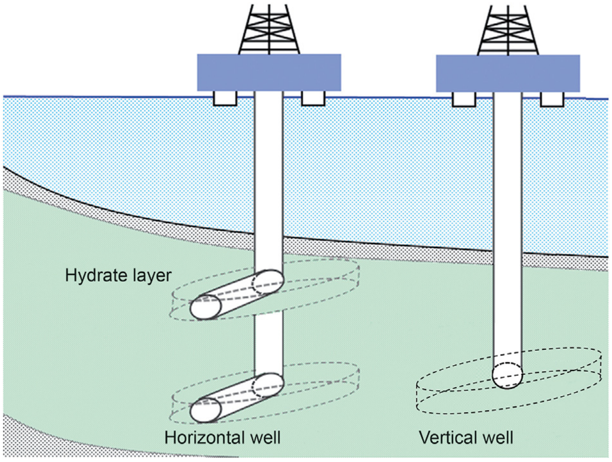

Fig. 8. Two types of wells for drilling hydrate reservoirs.

Table 2
Boundary stress parameters.

Parameter	Value		
Depth, meter below seafloor (mbsf)	200	400	600
Maximum horizontal ground stress, MPa	15.76	21.52	27.28
Minimum horizontal stress, MPa	14.33	19.56	24.80
Vertical geostress, MPa	19.70	26.90	34.10
Mud pressure, MPa	14.77	17.03	19.30
Pore pressure, MPa	14.50	16.50	18.50
Maximum horizontal effective in-situ stress, MPa	1.26	5.02	8.78
Minimum horizontal effective in-situ stress, MPa	−0.17	3.06	6.30
Vertical effective in-situ stress, MPa	5.20	10.40	15.60
Wellbore support stress, MPa	0.27	0.53	0.80

Table 3
Formation and drilling fluid physical parameters at Shenhu-2 station in Shenhu sea area, South China Sea, depth of 1235 m, 217.5 mbsf (Sun et al., 2018).

Paremeter	Value
Depth, mbsf	217.5
Pore pressure, MPa	14.689
Initial temperature, °C	14.178
Hydrate saturation, %	27
Pore water salinity, %	3.05
Drilling fluid pressure, MPa	14.975
Drilling fluid temperature, °C	15.2
Drilling fluid salinity, %	3.05

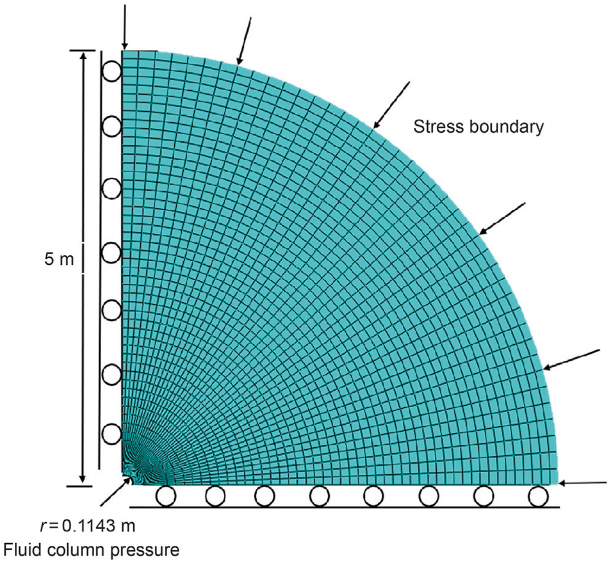

Fig. 9. The model of Sun et al. (2018).

been shown that the mechanical properties of a synthetic material made of circular cylinders is not a function of R/D (R is the particle size, D is the specimen width) value, provided that R/D is kept a small number (Potyondy and Cundall, 2004). In addition, in the study of Ding et al. (2014), they summarized the work of other scholars on particle size amplification. Following the research of the above scholars, we enlarged the particle size in the model to a certain extent.

Based on the model of Sun et al. the similar model was established (Fig. 10). In the wellbore stability of Fig. 2, the minimum radius of the sand particles is $R_{\text{sand-min}} = 0.04$ m, the maximum radius of the sand particles is $R_{\text{sand-max}} = 0.0664$ m, and the radius of all the hydrate particles $R_{\text{hyd}} = 0.04$ m. The dimension of the particles obeys the random distribution law and the particle size distribution is consistent with the above, the porosity is 0.15, and the width, height is 10 m, respectively. The X direction in the model is set as the direction of the vertical stress and the Y direction is set as the horizontal stress, in the middle of the model, a circular hole with radius of 0.1143 m was created for drilling mud invasion.

After the model was established, the drilling fluid invasion into the hydrate formation was studied using the parameters in Table 3 and compared with the results of Sun et al. (2018).

Fig. 11 compares the distribution of pore pressure around the well for our models and Sun et al.‘s model. The pore pressure obtained in this study is slightly lower, because the hydrate is assumed to be more stable and the temperature change of the formation in our work is relatively smaller. The results calculated by these two methods have the same trend and are the same when the point of interest is more than 0.5 m away from the borehole. Due to the decomposition of hydrate, the pore pressure of the formation near the wellbore wall is increased, while the pore pressure of the formation far away from the wellbore wall is still maintained the original value.

Fig. 12 compares the result of the radial length of the wellbore instability zone from the proposed model with solution given by Sun et al. The length of the instability zone calculated by the two methods has the same variation trend with time. The above comparison results verified the reliability and accuracy of the proposed morel in this paper.

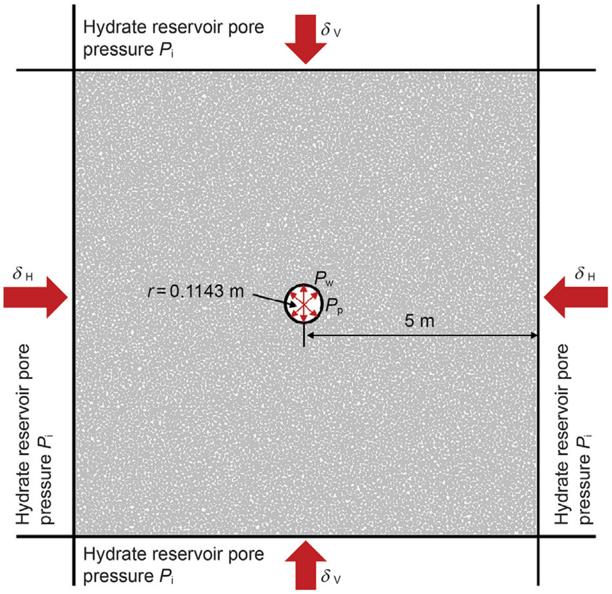

Fig. 10. Wellbore stability model.

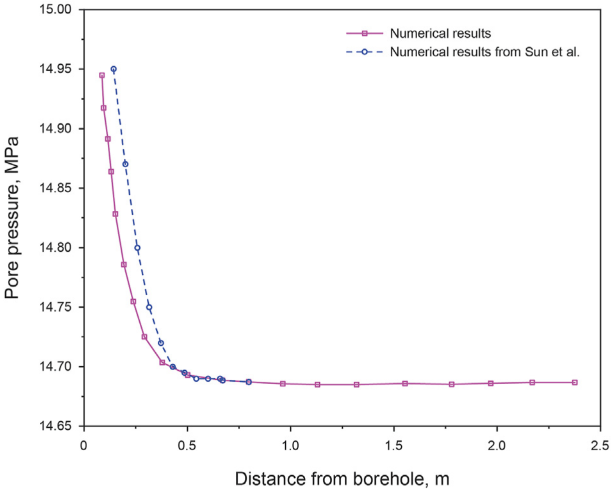

Fig. 11. Comparison of pore pressure changes.

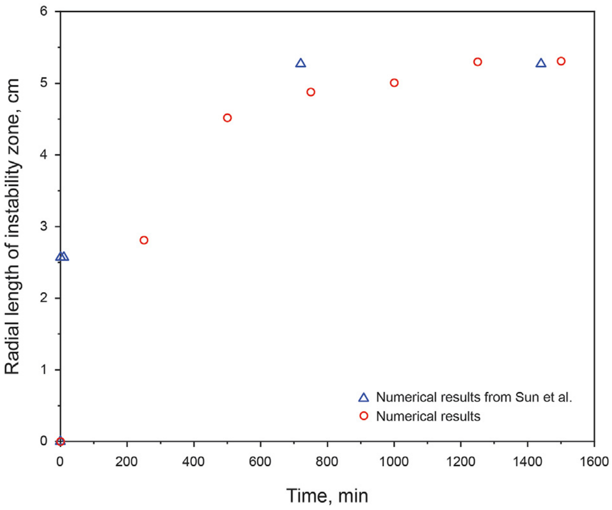

Fig. 12. Comparison of radial length of instability zone.

4. Results and discussion

According to the principle of hydraulic fracturing, this paper adopted the DEM to establish a numerical model to study the wellbore instability due to the seepage of drilling fluids into the hydrate with the parameters for the fluid calculation as listed Table 4. In this study, it is assumed that the temperature changes at the bottom of the well is small and thus the hydrate is relatively stable in the drilling process.

4.1. Influence of stress field difference on crack initiation and propagation

The pressure for drilling fluid invading into the hydrate formation was set as 8 MPa, and the minimum principal stress in the horizontal direction was maintained at 1 MPa. The stress difference in the horizontal direction was achieved by increasing the maximum principal stress. Fig. 13 shows the simulation results with different horizontal stress contrast. When the stress difference is relatively small (near homogenous stress condition in the horizontal direction), the fracture expansion length and intrusion area under constant hydraulic pressure are small and there is no obvious

Table 4
Fluid calculation parameters.

Residual aperture a_0, m	Fluid volume modulus K_f, Pa	Normal stress F, N	Range scaling factor, m	Timestep Δt, s	Permeability coefficient k, mm$\cdot$s^{-1}
2.0×10^{-3}	2.0×10^{9}	1.0×10^{6}	0.2	0.01	5.0×10^{-5}

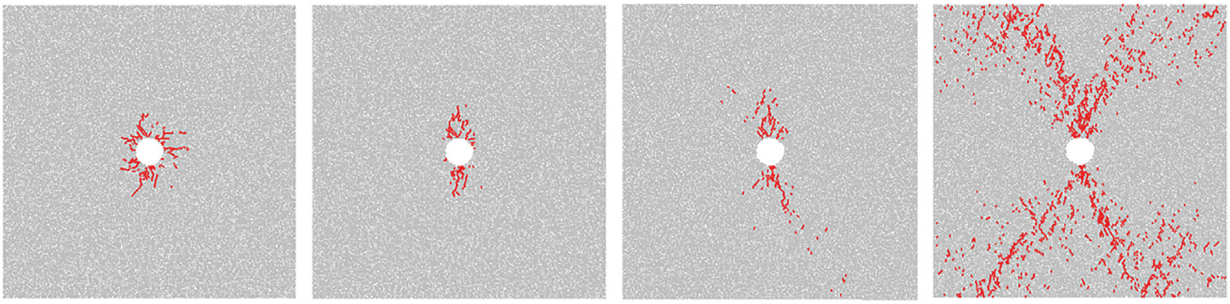
$\Delta\sigma = 0$ MPa $\Delta\sigma = 2$ MPa $\Delta\sigma = 4$ MPa $\Delta\sigma = 6$ MPa

Fig. 13. Final fracture geometries under different horizontal stress differences at an invasion pressure of 8 MPa.

favorable intrusion direction. With the increase of stress difference, the fracture growth direction tends to be parallel to the direction of the maximum horizontal principal stress (Duan et al., 2018; Shimizu et al., 2018). This is because when drilling fluid intrudes into hydrate bearing formation, it will take over the original particles and fluids of the formation. Since this process is carried out in a restricted pore space, the water content in this area will increase in the invasion process, resulting in a great pressure in local pores in this area and the formation of new fractures. According to the theory of fracture mechanics, the newly formed fracture tip has stress singularity, and the stress concentration at the fracture tip makes the failure strength of the rock there smaller than that of other areas, so the fluid pressure is more likely to accumulate and migrate at the fracture tip, thus promoting the continuous expansion of the fracture.

The distribution of the stress field around the borehole after fracture expansion is shown in Fig. 14. The stress value of the measurement circle is calculated as the average of all stress values on the contacts in the measuring circle instead of the stress value at a certain point. Due to discretization of the model particles, the stresses on each contact do not continuous, compared with the theoretical model with the uniform ideal conditions, the results from numerical model can reflect the real material performance better.

Due to the development of fractures, the height of pore pressure caused by hydrate decomposition, and the reconstruction of the initial stress field of the formation containing hydrate, the closer the wellbore, the more obvious the phenomenon of remodeling. Due to the induced fracture and pore pressure increase from hydrate decomposition, the stress field in the hydrate reconstructed. And this reconstruction is more obvious when it is closer to the fracture. It can be seen from Fig. 14, under different horizontal stress differences, the reconstructed stress field morphology of the hydrate formation is different, but the approximate variation of the stress field is similar. As the stress difference increases, the minimum horizontal principal stress of the direction is enhanced to a certain extent, and thus the stress at the tip of the fracture is weakened. A weak stress zone and a strong zone with obvious differences are formed inside the model.

4.2. Influence of invasion pressures on crack initiation and propagation

Fig. 15 shows the fracture propagation evolution under different invasion pressures with time. The maximum and minimum horizontal principal stresses are 5 MPa and 1 MPa, respectively. With the higher bottom hole pressure, the number of cracks increases. Micro fractures mainly extend in the direction of the maximum horizontal principal stress, and the extension in the direction of the minimum horizontal principal is suppressed. This is because the larger principal stress difference leads to the flow channel in one direction is relatively narrower and thus inhibit the drilling fluid invasion in the corresponding direction.

It can also be concluded from Fig. 15 that, in the same calculation time, the larger the intrusion fluid stress difference is, the longer the fracture will be, which also proves that the existence of the ground stress difference is an important factor determining the fracture expansion, and the existence of the stress difference can

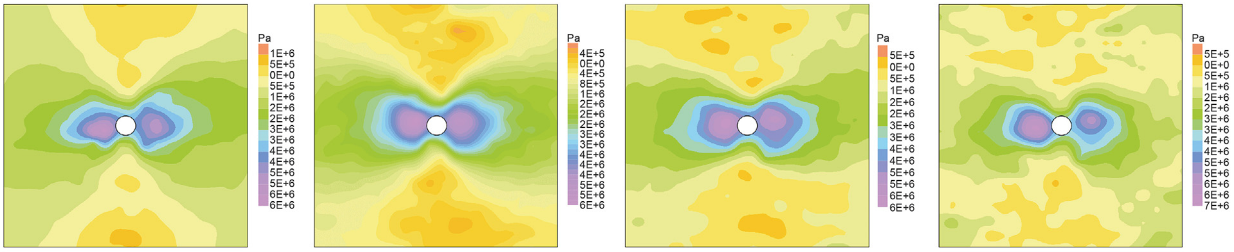

$\Delta\sigma = 0$ MPa $\Delta\sigma = 2$ MPa $\Delta\sigma = 4$ MPa $\Delta\sigma = 6$ MPa

Fig. 14. Distribution of the minimum horizontal principle stress field at an invasion pressure of 8 MPa.

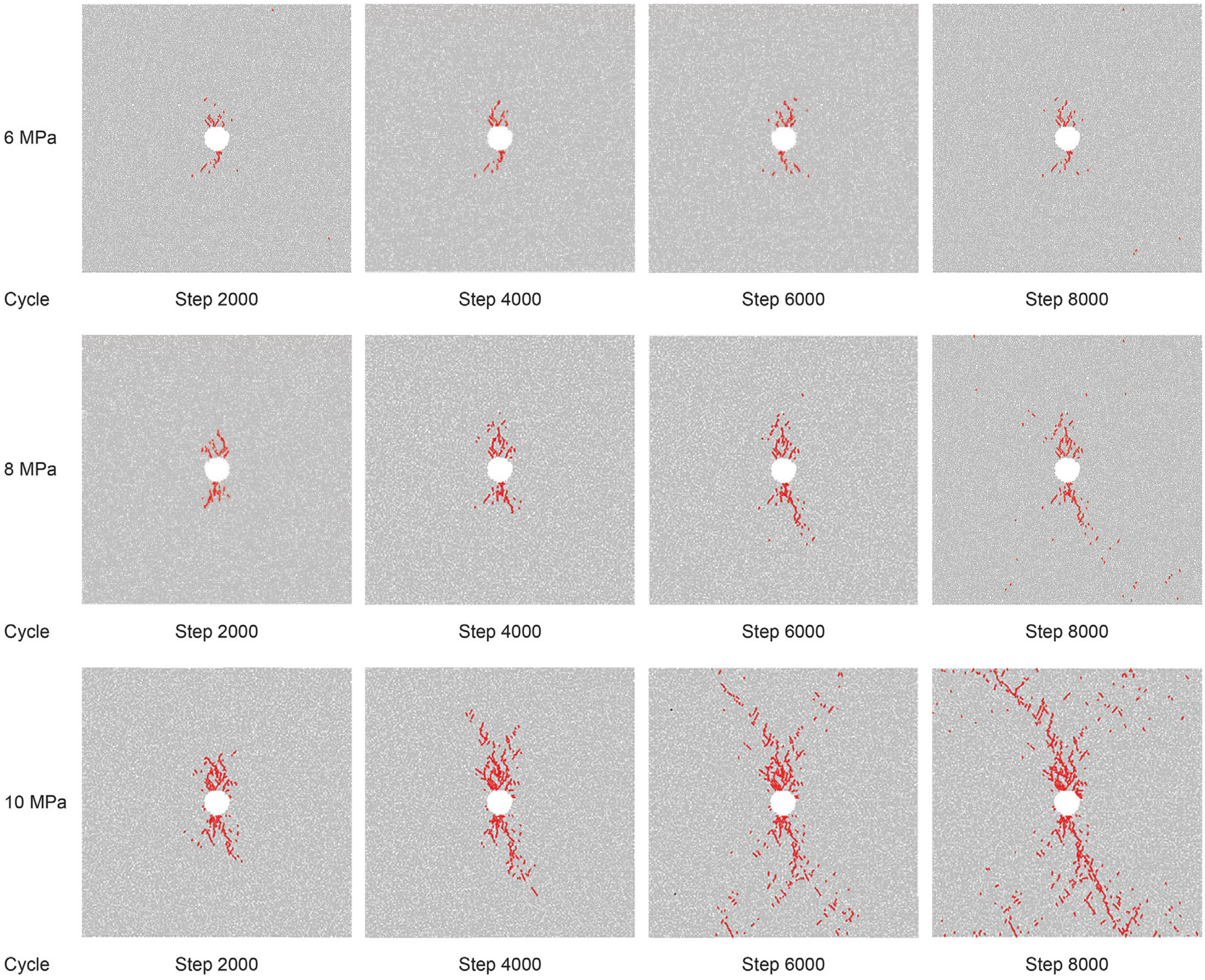

Fig. 15. Fracture propagation process at different invasion fluid pressures.

induce the (Rahmati et al., 2014; Tomac and Gutierrez, 2017) fracture expansion to some extent. In the simulation, the number of cracks in the formation in the invasion process was recorded as shown in Fig. 16. It is noticed that in Fig. 16, the starting value for *x*-axis (time axis) is not zero, and it is because the previous calculation steps are for model generation to reach the initial equilibrium stress state. As the pressure of the invading fluid increases, the rate of fracture propagation increases first and then decreases (curve slope). This trend is more pronounced for scenarios at low fluid pressure. When the fluid pressure is 6–8 MPa, the number of cracks first increases and then decreases and finally remains constant, and the expansion rate of the early micro fractures is small. As the pressure increases to 10 MPa, the rate of increase in the number of cracks also increases. The higher the pressure of the invading fluid, the faster the fracture growth rate. This phenomenon indicates that the invading fluid will form a network composed of micro fractures in the hydrate formation due to the hydraulic action, and the number of fractures will increase sharply at the beginning, and then the rate of fracture formation gradually slows down. The higher pressure of the invading fluid will result in more micro fractures formed in the hydrate with a faster rate, which is more conducive to the extension of fractures, which provides favorable conditions for the formation of the drilling fluid flow channel, but it is not good for the stability of wellbore.

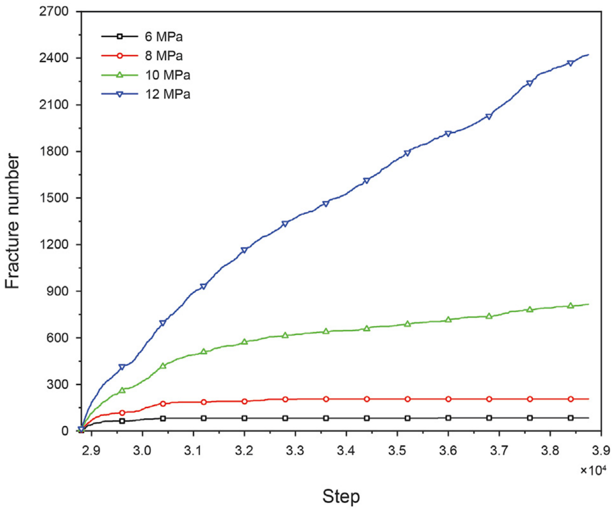

Fig. 16. Variation of fracture number at different invasion fluid pressures.

The rose diagram is often used to describe the distribution of fractures and their developmental intensity. It consists of linear coordinates and circular coordinates. The linear coordinate (in the radius direction) indicates the development strength of the fracture. The length of the petal depends on the frequency of investigated properties in the corresponding azimuth. The higher the frequency, the longer the length of the petal (Chong et al., 2017). The circular coordinate represents the azimuth angle of the fracture, which ranges from 0 to 360° and the minimum unit element is 20°. The azimuth angle of the fracture determines the flow direction of the drilling fluid. Both the azimuth and length of fracture are important parameters for fracture analysis. Intuitively, the direction of the petal on the rose diagram is consistent with the direction of the fracture in the hydrated stratigraphic zone. Meanwhile, the azimuth with more fractures (or higher density) has a longer length of the petal in the rose diagram.

Fig. 17 is the statistical result of fracture distribution orientation shown in the rose diagram. The distribution range of fracture azimuth, crack number and drilling fluid invasion area decrease with the decrease of invasion fluid pressure.

With an increase in the invasion fluid pressure, the density of micro fractures (the length of petals becomes longer) and the distribution range of the azimuth gradually increases. For example, when the invasion pressure is 6 MPa, the range of the azimuth angle of the fracture is 5°–155°, and the fracture number is 24. While the pressure of the intrusion fluid increases to 12 MPa, the range of the azimuth angle of the fracture is 0°–180°, and the fracture number is 514. Compared with the low invasion fluid pressure, the azimuth angle range of the micro fracture is wider, the azimuth angle range of the fracture is enlarged by about 40°, and the density of the micro fracture also increases greatly. Compared with the invasion fluid pressure of 6 MPa, the density of the micro fracture increases by 490.

The above conclusion indicates that higher fluid invasion pressure will cause more cracks in a wider range of direction as what also suggested in Fig. 17.

4.3. Influence of hydrate saturation difference on crack initiation and propagation

Three models with different saturation (S_h = 30%, S_h = 40%, S_h = 50%) were considered to study the effect hydrate saturation on the fracture propagation of the drilling fluid in the hydrate formation. The minimum horizontal principal stress is 1 MPa, the maximum horizontal principal stress is 3 MPa, and the pressure of the invasion fluid is 8 MPa in these three models.

Fig. 18 shows the final expanded morphology of the area invaded by the drilling fluid at different saturations, which indicates that lower hydrate saturation will result in more cracks produced and more fracture propagation paths.

Fig. 19 shows the variation of the crack number versus time at different hydrate saturation values. The number of cracks decreases with an increase in hydrate saturation. While when the hydrate saturation increases from 30% to 50%, the decrease in the crack number is about 60%. Hydrate saturation is also an important factor affecting fracture propagation. Fig. 19 also suggests that the fracture propagation rate in the low saturation formation is higher than high hydrate saturation formation. The hydrate can enhance the mechanical properties of the formation, the mechanical properties increases with increasing hydrate saturation (Zhu et al., 2018). Therefore, the formation with lower hydrate saturation can produce more cracks, and the fluid is easier to invade.

Fig. 20 shows the breakdown pressure versus time at the hydrate saturation of 50%. The pressure in the pore gradually increases from the initial value to the peak, and then it drops sharply. At beginning, the drilling fluid invades the hydrate and cause the pressure to increase; after the fracture is initiated and propagated, the drilling fluid will flow into the induced fracture, and the pressure in the hole decreases (Chen et al., 2018). This peak is the breakdown pressure. As the fractures are generated, the drilling fluid continues to flow into the resulting fracture passages, causing the pressure in the bore to continue to decrease and eventually remain substantially constant.

Table 5 shows the breakdown pressure of the hydrate formation at different degrees of hydrate saturation. As the hydrate saturation increases, the breakdown pressure gradually increases. The degree of formation consolidation is relatively poor at the lower hydrate saturation. In addition, combined with the above analysis of the

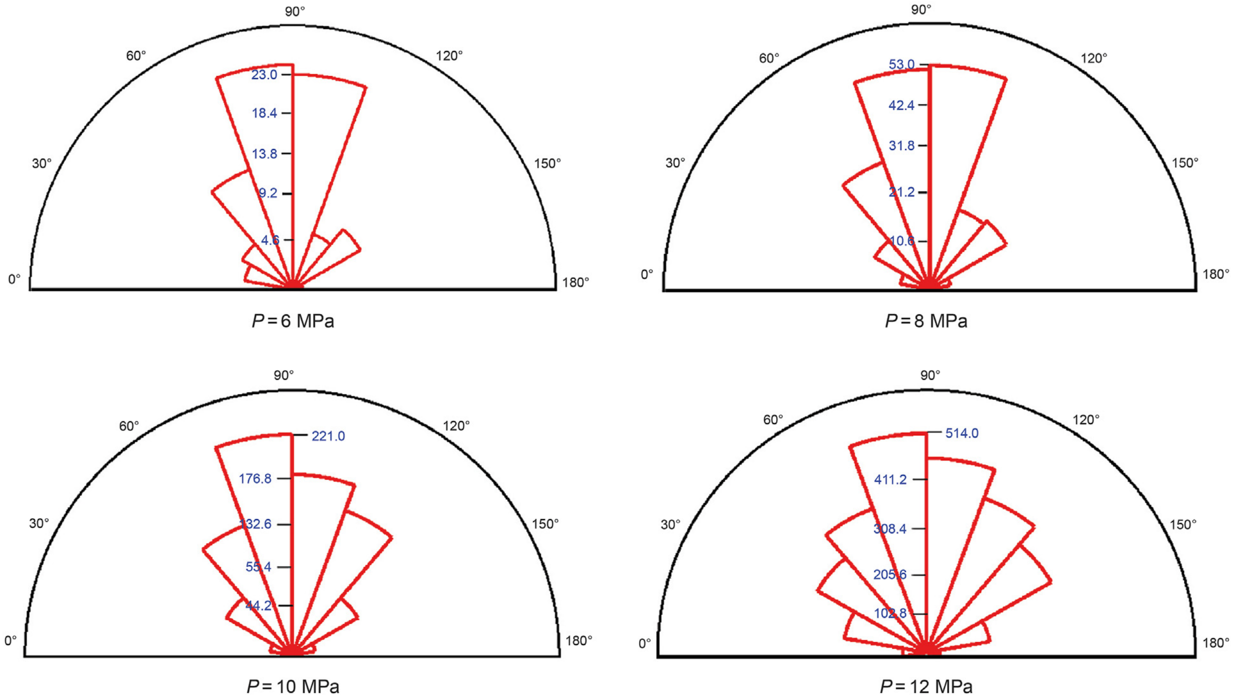

$P = 6$ MPa

$P = 8$ MPa

$P = 10$ MPa

$P = 12$ MPa

Fig. 17. Rose diagram of fracture distribution at different invasion pressures.

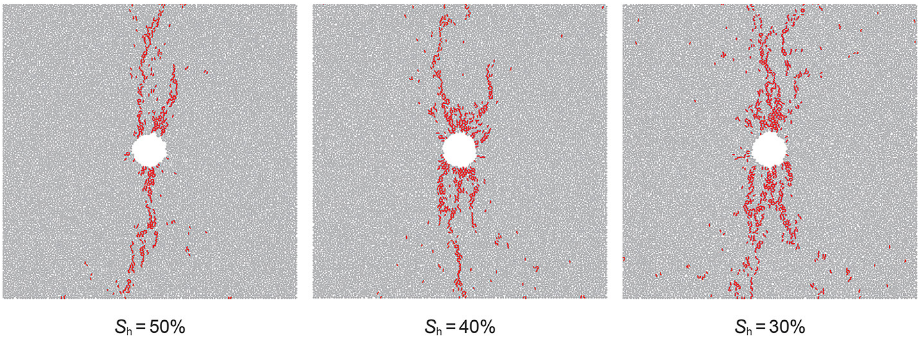

$S_h = 50\%$ $S_h = 40\%$ $S_h = 30\%$

Fig. 18. Final expansion of fractures at different hydrate saturations.

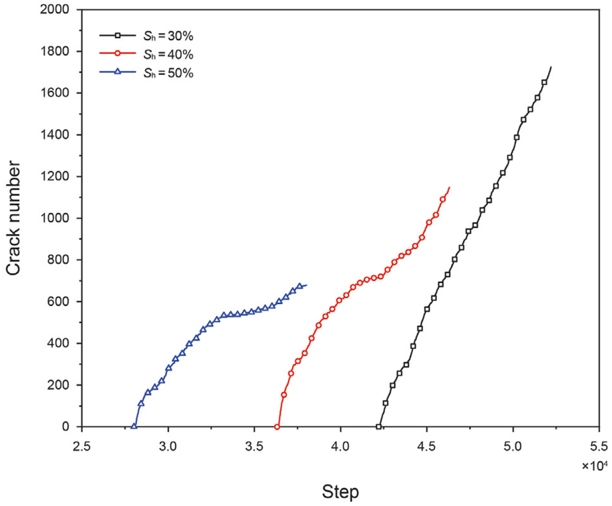

Fig. 19. Curve of the number of cracks with time at different hydrate saturation values.

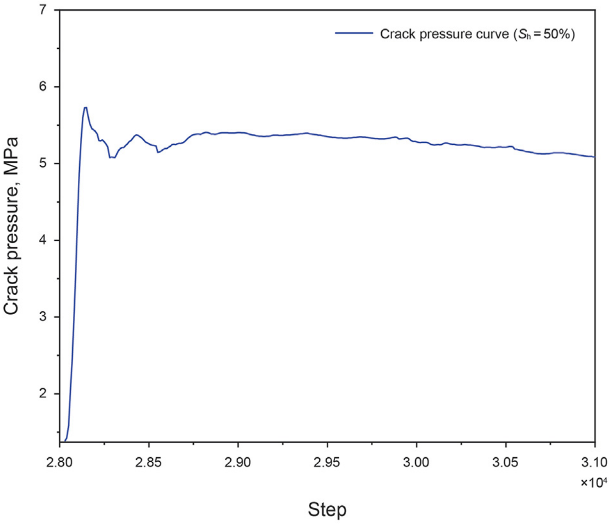

Fig. 20. Curve of fracture pressure with time when the hydrate saturation is 50%.

Table 5
Formation fracture pressure at different hydrate saturations.

Saturation, %	Breakdown pressure, MPa
50	5.73
40	4.91
30	4.83

stress field, for the formation with lower saturation, it is easier to release stress due to non-compaction in some areas, so the breakdown pressure is lower.

4.4. Analysis of borehole stability at different seabed depths

The boundary conditions are set to analyze the fracture propagation and the formation stress distribution at different sea-depth. It can be seen from Fig. 21 that the stress field around the wellbore is reconstructed after loading. For 200 m below seabed, the change of the maximum horizontal principal stress in the influenced area is relatively small and is increased by 0.8 MPa. Most of the investigated domain has not been affected except the vicinity of the fracture. Compared with the change of the maximum horizontal principal stress, the change of the minimum horizontal principal stress in the influenced area is very large, the pressure near the borehole is about 1 MPa. The stress field reconstruction is more obvious around the borehole. When the formation is 400 m and 600 m below the seabed, the change of the stress field is smaller than that of at 200 m.

The final fracture growth pattern (Fig. 22a) and the percolation area of the drilling fluid (Fig. 22b). This indicate that when the depth is relatively deep (600 mbsf), the fracture distribution is mainly concentrated around the wellbore and does not extend forward into the formation. As the formation depth becomes shallower, the fracture length increases and the drilling fluid invasion area also increases. This is because with the formation depth gets deeper, the stress difference gradually decreases and the fracture is not easy to expand.

5. Conclusions

Based on the principle of hydraulic fracturing, the authors use the DEM to simulate the influence of drilling fluid invasion into the hydrate formation on the stability of the borehole from the perspective of crack initiation and propagation. The following conclusions are drawn:

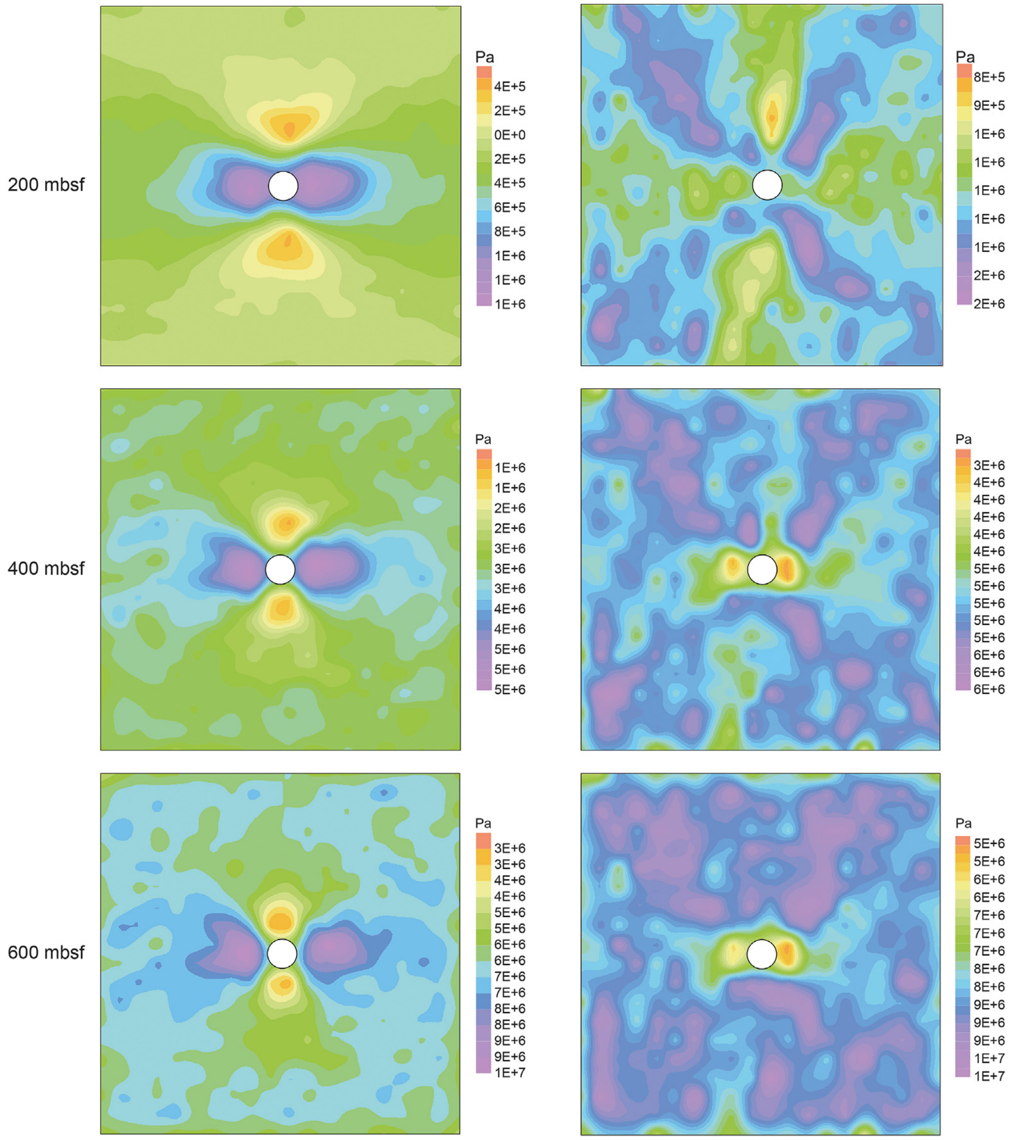

(a) Minimum horizontal principal stress distribution

(b) Maximum horizontal principal stress distribution

Fig. 21. Distribution of final stress field at different depths.

(1) Numerical simulation results show that the difference in in-situ stresses has an important effect on the initiation of cracks during the invasion of drilling fluid into the hydrate formation. Due to the influence of the difference in in-situ stress, the fracture always propagates toward the direction of the maximum horizontal stress, and the extension of the fracture in the direction of the minimum horizontal stress is suppressed. The small stress difference will produce disorderly cracks, and the large stress difference will produce planar cracks. As the fracture propagates, the stress at the fracture tip gradually decreases.

(2) The formation of micro-fractures is faster at a higher invasion pressure of the drilling fluid, which is more conducive to the extension of fractures and provides favorable conditions for the formation of drilling fluid flow channels.

(3) Because the hydrate can enhance the mechanical properties of the formation, under the same invasion fluid pressure, the formation with lower hydrate saturation can produce more cracks, and the fluid is easier to invade. Meanwhile, the breakdown pressure increases with the increase of the hydrate saturation.

(4) As the depth increases, the stress field around the wellbore experiences a more recognizable reconstructed in both amplitude and scope. When the depth is 600 mbsf, random cracks are formed near the wellbore, and the cracks do not propagate forward into the formation. As the formation depth becomes shallower, it is easier to form a planar fracture and the area of drilling fluid invasion will be larger.

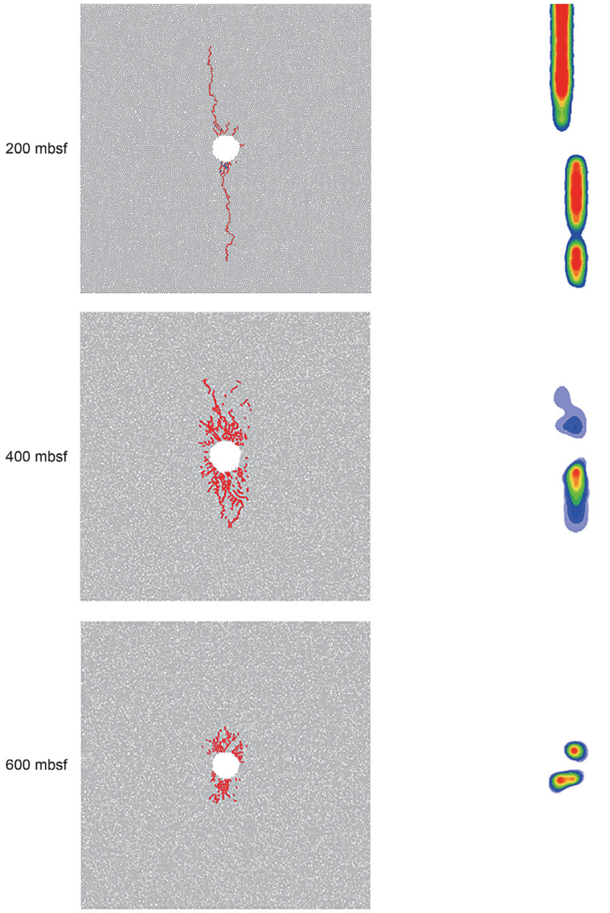

(a) Final fractures

(b) Fluid seepage area

Fig. 22. Final fracture propagation and drilling fluid invasion at different depths.

Acknowledgements

This research project is funded by National Natural Science Foundation of China (No. 51874253, No. U19A2097, U20A20265), and the National Key R&D Program of China (No. 2018YFC0310200). The authors also sincerely appreciate the editors and the reviewers for the efforts in improving this paper, and Prof. Fengshou Zhang for providing the PFC code.

References

Bahrani, N., Kaiser, P.K., Valley, B., 2014. Distinct element method simulation of an analogue for a highly interlocked, non-persistently jointed rock mass. Int. J. Rock Mech. Min. Sci. 71, 117–130. https://doi.org/10.1016/j.ijrmms.2014.07.005.

Berman, A.S., 1953. Laminar flow in channels with porous walls. J. Appl. Phys. 24 (9), 1232–1235. https://doi.org/10.1063/1.1721476.

Birchwood, R.A., Noeth, S., Tjengdrawira, M.A., et al., 2007. Modeling the mechanical and phase change stability of wellbores drilled in gas hydrates by the joint industry participation program (JIP) gas hydrates project, Phase II. In: SPE Annual Technical Conference and Exhibition. Society of Petroleum Engineers. https://doi.org/10.2118/110796-MS.

Castro-Filgueira, U., Alejano, L.R., Arzúa, J., et al., 2017. Sensitivity analysis of the micro-parameters used in a PFC analysis towards the mechanical properties of rocks. Procedia Engineering 191, 488–495. https://doi.org/10.1016/j.proeng.2017.05.208.

Chen, W., Konietzky, H., Liu, C., et al., 2018. Hydraulic fracturing simulation for heterogeneous granite by discrete element method. Comput. Geotech. 95, 1–15. https://doi.org/10.1016/j.compgeo.2017.11.016.

Cho, N., Martin, C.D., Sego, D.C., 2007. A clumped particle model for rock. Int. J. Rock Mech. Min. Sci. 44, 997–1010. https://doi.org/10.1016/j.ijrmms.2007.02.002.

Chong, Z.H., Karekal, S., Li, X.H., et al., 2017. Numerical investigation of hydraulic fracturing in transversely isotropic shale reservoirs based on the discrete element method. J. Nat. Gas Sci. Eng. 46, 398–420. https://doi.org/10.1016/j.jngse.2017.08.021.

Chong, Z.R., Zhao, J., Chan, J.H.R., et al., 2018. Effect of horizontal wellbore on the production behavior from marine hydrate bearing sediment. Appl. Energy 214, 117–130. https://doi.org/10.1016/j.apenergy.2018.01.072.

Cundall, P.A., Strack, O.D., 1979. A discrete numerical model for granular assemblies. Geotechnique 29 (1), 47–65. https://doi.org/10.1680/geot.1979.29.1.47.

Ding, X.B., Zhang, L.Y., Zhu, H.H., et al., 2014. Effect of model scale and particle size distribution on PFC3D simulation results. Rock Mech. Rock Eng. 47, 2139–2156. https://doi.org/10.1007/s00603-013-0533-1.

Duan, K., Kwok, C.Y., Wu, W., et al., 2018. DEM modeling of hydraulic fracturing in permeable rock: influence of viscosity, injection rate and in situ states. Acta Geotechnica 13 (5), 1187–1202. https://doi.org/10.1007/s11440-018-0627-8.

Freij-Ayoub, R., 2008. Wellbore stability issues in shales or hydrate bearing sediments. SPE Distinguished Lecturer Series. https://www.spe.org/dl/docs/2008/Freij-Ayoub.pdf.

Freij-Ayoub, R., Tan, C., Clennell, B., et al., 2007. A wellbore stability model for hydrate bearing sediments. J. Petrol. Sci. Eng. 57 (1–2), 209–220. https://doi.org/10.1016/j.petrol.2005.10.011.

Hofmann, H., Babadagli, T., Yoon, J.S., et al., 2015. A grain based modeling study of mineralogical factors affecting strength, elastic behavior and micro fracture development during compression tests in granites. Eng. Fract. Mech. 147, 261–275. https://doi.org/10.1016/j.engfracmech.2015.09.008.

Huang, L.K., Liu, J.J., Zhang, F.S., et al., 2019. Exploring the influence of rock inherent heterogeneity and grain size on hydraulic fracturing using discrete element modeling. Int. J. Solid Struct. 176, 207–220. https://doi.org/10.1016/j.ijsolstr.2019.06.018.

Itasca Consulting Group, I., 2008. PFC 3D Version 4.0. Itasca, Minneapolis, MN.

Khabibullin, T., Falcone, G., Teodoriu, C., 2011. Drilling through gas-hydrate sediments: managing wellbore-stability risks. SPE Drill. Complet. 26 (2), 287–294. https://doi.org/10.2118/131332-PA.

Li, D.Q., 2014. Underground hydraulic mining of thin sub-layer as protective coal seam in coal mines. International Journal Of Rock Mechanics and Mining Sciences 67, 145–154. https://doi.org/10.1007/s11069-013-0898-1.

Li, L., Cheng, Y., Zhang, Y., et al., 2011. A fluid-solid coupling model of wellbore stability for hydrate bearing sediments. Procedia Engineering 18, 363–368. https://doi.org/10.1016/j.proeng.2011.11.058.

Lisjak, A., Grasselli, G., 2014. A review of discrete modeling techniques for fracturing processes in discontinuous rock mass. Journal of Rock Mechanics and Geotechnical Engineering 6, 301–314. https://doi.org/10.1016/j.jrmge.2013.12.007.

Liu, W.R., 2017. Mechanical Characteristics and the Shell Formation Mechanism of the Force Chain of Surrounding Rock in Stope. AnHui University of Science and Technology (in Chinese). https://kns.cnki.net/kcms/detail/detail.aspx?FileName=1017171815.nh&DbName=CDFD2017.

Liu, Y.Q., Li, H.B., Luo, C.W., et al., 2014. In situ stress measurements by hydraulic fracturing in the Western route of South to North water transfer project in China. Eng. Geol. 168, 114–119. https://doi.org/10.1016/j.enggeo.2013.11.008.

Liu, X.L., Wang, S.J., Wang, S.Y., et al., 2015. Fluid-driven fractures in granular materials. Bull. Eng. Geol. Environ. 74 (2), 621–636. https://doi.org/10.1007/s10064-014-0712-7.

Lönnqvist, M., Hökmark, H., 2016. Thermal, mechanical and thermo-mechanical assessment of the rock mass surrounding SKB's prototype repository at Äspö HRL. Rock Mech. Rock Eng. 49, 1123–1142. https://doi.org/10.1007/s00603-015-0809-8.

McConnell, D.R., Zhang, Z.J., Boswell, R., 2012. Review of progress in evaluating gas hydrate drilling hazards. Mar. Petrol. Geol. 34 (1), 209–223. https://doi.org/10.1016/j.marpetgeo.2012.02.010.

Merey, S., 2016. Drilling of gas hydrate reservoirs. J. Nat. Gas Sci. Eng. 35, 1167–1179. https://doi.org/10.1016/j.jngse.2016.09.058.

Nasehi, M.J., Mortazavi, A., 2013. Effects of in-situ stress regime and intact rock strength parameters on the hydraulic fracturing. J. Petrol. Sci. Eng. 108, 211–221. https://doi.org/10.1016/j.petrol.2013.04.001.

Ning, F.L., Wu, N.Y., Yu, Y.B., et al., 2013a. Invasion of drilling mud into gas-hydrate-bearing sediments. Part II: effects of geophysical properties of sediments. Geophys. J. Int. 193 (3), 1385–1398. https://doi.org/10.1093/gji/ggt016.

Ning, F.L., Zhang, K.N., Wu, N.Y., et al., 2013b. Invasion of drilling mud into gas-hydrate-bearing sediments. Part I: effect of drilling mud properties. Geophys. J. Int. 193 (3), 1370–1384. https://doi.org/10.1093/gji/ggt016.

Pogacnik, J., Elsworth, D., O'Sullivan, M., et al., 2016. A damage mechanics approach to the simulation of hydraulic fracturing/shearing around a geothermal injection well. Comput. Geotech. 71, 338–351. https://doi.org/10.1016/j.compgeo.2015.10.003.

Potyondy, D.O., Cundall, P.A., 2004. A bonded-particle model for rock. Int. J. Rock Mech. Min. Sci. 41 (8), 1329–1364. https://doi.org/10.1016/j.ijrmms.2004.09.011, 2004.

Rahmati, H., Nouri, A., Chan, D., et al., 2014. Simulation of drilling-induced compaction bands using discrete element method. Int. J. Numer. Anal. Methods GeoMech. 38 (1), 37–50. https://doi.org/10.1002/nag.2194.

Rutqvist, J., Moridis, G., Grover, T., et al., 2012. Coupled multiphase fluid flow and wellbore stability analysis associated with gas production from oceanic hydrate-bearing sediments. J. Petrol. Sci. Eng. 92, 65–81. https://doi.org/10.1016/j.petrol.2012.06.004.

Shimizu, H., Murata, S., Ishida, T., 2011. The distinct element analysis for hydraulic fracturing in hard rock considering fluid viscosity and particle size distribution.

Int. J. Rock Mech. Min. Sci. 48 (5), 712–727. https://doi.org/10.1016/j.ijrmms.2011.04.013.

Shimizu, H., Ito, T., Tamagawa, T., et al., 2018. A study of the effect of brittleness on hydraulic fracture complexity using a flow-coupled discrete element method. J. Petrol. Sci. Eng. 160, 372–383. https://doi.org/10.1016/j.petrol.2017.10.064.

Sloan, E.D., 2003. Fundamental principles and applications of natural gas hydrates. Nature 426 (6964), 353–359. https://doi.org/10.1038/nature02135.

Sun, J.X., Ning, F.L., Wu, N.Y., et al., 2015. The effect of drilling mud properties on shallow lateral resistivity logging of gas hydrate bearing sediments. J. Petrol. Sci. Eng. 127, 259–269. https://doi.org/10.1016/j.petrol.2014.12.015.

Sun, J.X., Ning, F.L., Lei, H.W., et al., 2018. Wellbore stability analysis during drilling through marine gas hydrate-bearing sediments in Shenhu area: a case study. J. Petrol. Sci. Eng. 170, 345–367. https://doi.org/10.1016/j.petrol.2018.06.032.

Tomac, I., Gutierrez, M., 2017. Coupled hydro-thermo-mechanical modeling of hydraulic fracturing in quasi-brittle rocks using BPM-DEM. Journal of Rock Mechanics and Geotechnical Engineering 9 (1), 92–104. https://doi.org/10.1016/j.jrmge.2016.10.001.

Wang, C.H., Song, C.K., Guo, Q.L., et al., 2015. New insights into stress changes before and after the Wenchuan Earthquake using hydraulic fracturing measurements. Eng. Geol. 194, 98–113. https://doi.org/10.1016/j.enggeo.2015.05.016.

Wang, L.Z., Wang, G.R., Mao, L.J., et al., 2020. Experimental research on the breaking effect of natural gas hydrate sediment for water jet and engineering applications. J. Petrol. Sci. Eng. 184, 106553. https://doi.org/10.1016/j.petrol.2019.106553.

Wojtanowicz, A.K., Bourgoyne, A.T., Zhou, D., et al., 2000. Strength and Fracture Gradients for Shallow Marine Sediments. US Department of Interior Mineral Management Service. Final Report. https://www.bsee.gov/sites/bsee.gov/files/tap-technical-assessment-program//008dj.pdf.

Wu, N., Zhang, H., Su, X., et al., 2007. High concentrations of hydrate in disseminated forms found in very fine-grained sediments of Shenhu area, South China Sea. Terra Nostra (Bonn) 1 (2), 236–237. https://www.researchgate.net/publication/285023322.

Yan, C.L., Cheng, Y.F., Li, M.L., et al., 2017. Mechanical experiments and constitutive model of natural gas hydrate reservoirs. Int. J. Hydrogen Energy 42 (31), 19810–19818. https://doi.org/10.1016/j.ijhydene.2017.06.135.

Yoon, J.S., Zang, A., Stephansson, O., 2014. Numerical investigation on optimized stimulation of intact and naturally fractured deep geothermal reservoirs using hydro-mechanical coupled discrete particles joints model. Geothermics 52, 165–184. https://doi.org/10.1016/j.geothermics.2014.01.009.

Yoon, J.S., Zimmermann, G., Zang, A., 2015. Numerical investigation on stress shadowing in fluid injection-induced fracture propagation in naturally fractured geothermal reservoirs. Rock Mech. Rock Eng. 48 (4), 1439–1454. https://doi.org/10.1007/s00603-014-0695-5.

Zhang, H.Q., Yang, S., Wu, N., et al., 2007. Successful and surprising results for China's first gas hydrate drilling expedition. Fire Ice Newsl.: Methane Hydrate Newsl 7 (3), 6–9. https://www.researchgate.net/publication/286200076.

Zhang, C.Y., Chen, Q.C., Fan, T., et al., 2015. Deep-hole in situ stress measurement of Xisha islands and analysis of its tectonic significance. In: The 17th Annual Meeting of China Association for Science and Technology-Proceedings of 9 Symposium on Deepwater Oil and Gas Exploration and Development Technology in the South China Sea (in Chinese). https://kns.cnki.net/kcms/detail/detail.aspx?FileName=DIDD201505008004&DbName=CPFD2015.

Zhou, J., Huang, H., Deo, M., 2015. Modeling the interaction between hydraulic and natural fractures using dual-lattice discrete element method. In: 49th US Rock Mechanics/Geomechanics Symposium. American Rock Mechanics Association. In: https://onepetro.org/ARMAUSRMS/proceedings-abstract/ARMA15/All-ARMA15/ARMA-2015-507/65877.

Zhou, J., Zhang, L.Q., Pan, Z.J., et al., 2016. Numerical investigation of fluid-driven near-borehole fracture propagation in laminated reservoir rock using PFC2D. J. Nat. Gas Sci. Eng. 36, 719–733. https://doi.org/10.1016/j.jngse.2016.11.010.

Zhu, H.Y., Liu, Q.Y., Deng, J.G., et al., 2011. Pressure and temperature preservation techniques for gas-hydrate-bearing sediments sampling. Energy 36 (7), 4542–4551. https://doi.org/10.1016/j.energy.2011.03.053.

Zhu, H.Y., Liu, Q.Y., Wong, G.R., et al., 2013. A pressure and temperature preservation system for gas-hydrate-bearing sediments sampler. Petrol. Sci. Technol. 31 (6), 652–662. https://doi.org/10.1080/10916466.2010.531352.

Zhu, H.Y., Shen, J.D., Zhang, F.S., et al., 2018. Nonlinear constitutive model and discrete-element-method modeling of synthetic methane hydrate sand. In: 52nd US Rock Mechanics/Geomechanics Symposium. American Rock Mechanics Association. In: https://onepetro.org/ARMAUSRMS/proceedings-abstract/ARMA18/All-ARMA18/ARMA-2018-1049/124058.